Principles of Aboveground Biomass Estimation via Remote Sensing

Subjects: Forestry

Contributor: Lei Tian , Xiaocan Wu , Yu Tao , Mingyang Li , Chunhua Qian , Longtao Liao , Wenxue Fu

Quantifying forest aboveground biomass (AGB) is essential for elucidating the global carbon cycle and the response of forest ecosystems to climate change. Remote-sensing techniques have played a vital role in forest AGB estimation at different scales.

forest aboveground biomass optical remote sensing remote sensing

1. Introduction

The rapidly changing climate has severely impacted natural ecosystems and human societies worldwide, resulting in a series of ecological issues, including rising global sea levels [1], accelerated glacial melting at high latitudes and elevations [2][3][4], extremely severe weather [5][6], reduced food production [7], species extinction [8], and deleterious human health effects [9] which directly threaten the survival and security of human beings [10]. Global climate change imposes serious, long-term challenges to the sustainable development of human societies and has evolved into a political, economic, and environmental issue of global concern [11][12].

Forest ecosystems comprise the largest terrestrial carbon pool, storing approximately 76%–98% of terrestrial organic carbon (approximately 80% of above- and 40% of belowground carbon) [13][14]. Moreover, forest ecosystems play a crucial role in the global carbon cycle by absorbing greenhouse gases (GHG) such as atmospheric CO_2, thereby reducing GHG concentrations and mitigating global climate change [15][16][17][18].

Forest aboveground biomass (AGB, the aboveground part of forest biomass) reflects the complicated relationship between the nutrient cycle and energy flow [19], providing the necessary nutrient sources and energy base for the functionality of the entire forest ecosystem [20]. In addition, AGB is a key indicator of forest ecosystem carbon sequestration capacity [21][22], productivity, structural function [23][24], and carbon sources and sinks [21][25][26]. Forest AGB estimates have been used as surrogates for aboveground carbon measurements [27]. Accordingly, AGB variations reflect the quality and condition of forest ecosystems [28][29], as well as the effects of ecological succession, natural disturbances, human activities, and climate change on forests [21][30][31]. Therefore, forest AGB estimations in the context of climate change could provide a theoretical basis for the study of the carbon cycle in terrestrial ecosystems and global climate change [18][22][32], which plays a crucial role in understanding and monitoring the response of forest ecosystems to GHG emissions [13][28][33]. In addition, the estimation of forest AGB has contributed to providing strategic guidelines for sustainable forest management [24][34], as well as rational utilization of forest resources and improvement of the forest ecological environment [14][28][29][35].

A rapid and accurate estimation of forest AGB remains challenging in forestry research [25][30]. In general, forest AGB estimation methods can be categorized as field measurements, remote sensing-based approaches, and ecological model simulations [25][36]. Field measurements entail the construction of allometric equations using tree height and diameter data measured via National Forest Inventory (NFI) data or auxiliary field plots [19][37][38][39]. To date, field measurements are considered the most accurate means of obtaining forest biomass data [19][40]; however, these measurements are also the most challenging on a regional scale because of the lengthy and arduous nature of ground-based measurements [30][41]. In addition, the actual amount of land inventoried tends to be quite small; for example, the United States Department of Agriculture (USDA) Forest Service Forest Inventory and Analysis program uses 1 plot per 2400 ha of land. Alternatively, remote sensing-based approaches combine ground measurement data with remotely sensed data to estimate parameters that highly correlate with AGB. This is achieved by obtaining spectral features and vegetation metrics from multi-source remotely sensed data, such as vegetation indices (VIs), canopy cover and height, texture, shaded fraction, leaf and basal area, and timber volume [31][42][43][44][45], whereafter an AGB estimation model is constructed for regional AGB mapping [37]. In addition to the two aforementioned methods, ecological model simulation is a promising tool for the dynamic assessment of regional AGB [46]. However, this approach is often location-specific, has poor applicability, and requires a large number of input parameters for which appropriate values may be difficult to obtain [47][48]. Therefore, remote sensing-based approaches remain the dominant data source for AGB mapping and estimation in different environments [30][36][49][50].

Optical remote sensing images with varying spatial, spectral, and temporal resolutions are freely available and are widely used to estimate AGB at different scales [49][51][52]. For example, moderate- and coarse-resolution data, such as those obtained from the moderate resolution imaging spectroradiometer (MODIS), are typically employed in large-scale AGB estimates for global, continental, or national regions [53][54]. Conversely, medium-resolution data, such as those obtained from Sentinel-2 and Landsat, are mainly used to estimate AGB at local scales [55][56][57][58]. Finer-resolution commercial satellite data, such as those obtained from IKONOS, QuickBird, and WorldView-2, have been employed for AGB estimation at the forest stand scale [59][60][61]. In addition, microwave radar remotely sensed data, including synthetic aperture radar (SAR), interferometric SAR (InSAR), and polarimetric InSAR (PolInSAR) data, have also been used to estimate AGB at regional scales with moderate spatial resolutions [62][63][64][65][66]. However, optical and radar data generally suffer from signal saturation at high AGB, which limits their ability to estimate AGB in dense tropical and subtropical forests [40][67]. Recently, measurements collected using LiDAR, which is capable of acquiring tree height, canopy area, and stand density data, have improved AGB estimations in dense forests [68][69]. Furthermore, unmanned aerial vehicles (UAVs) have emerged as promising remote sensing tools over the last few decades, demonstrating enhanced applications in forest AGB estimation [70][71][72][73].

2. Principles of AGB Estimation via Remote Sensing

As opposed to direct forest biomass estimations, remote sensing techniques generally evaluate forest AGB through the construction and use of parameters such as optical sensor-derived surface reflectance, VIs, leaf area index

(LAI), coverage, and tree and canopy height, with the aim to establish relationships that serve as a proxy for the AGB [36]. The remote sensing techniques used to estimate forest AGB are illustrated in **Figure 1**. Over the past decades, remote sensing has played a critical role in estimating forest AGB at various spatial and temporal scales [18].

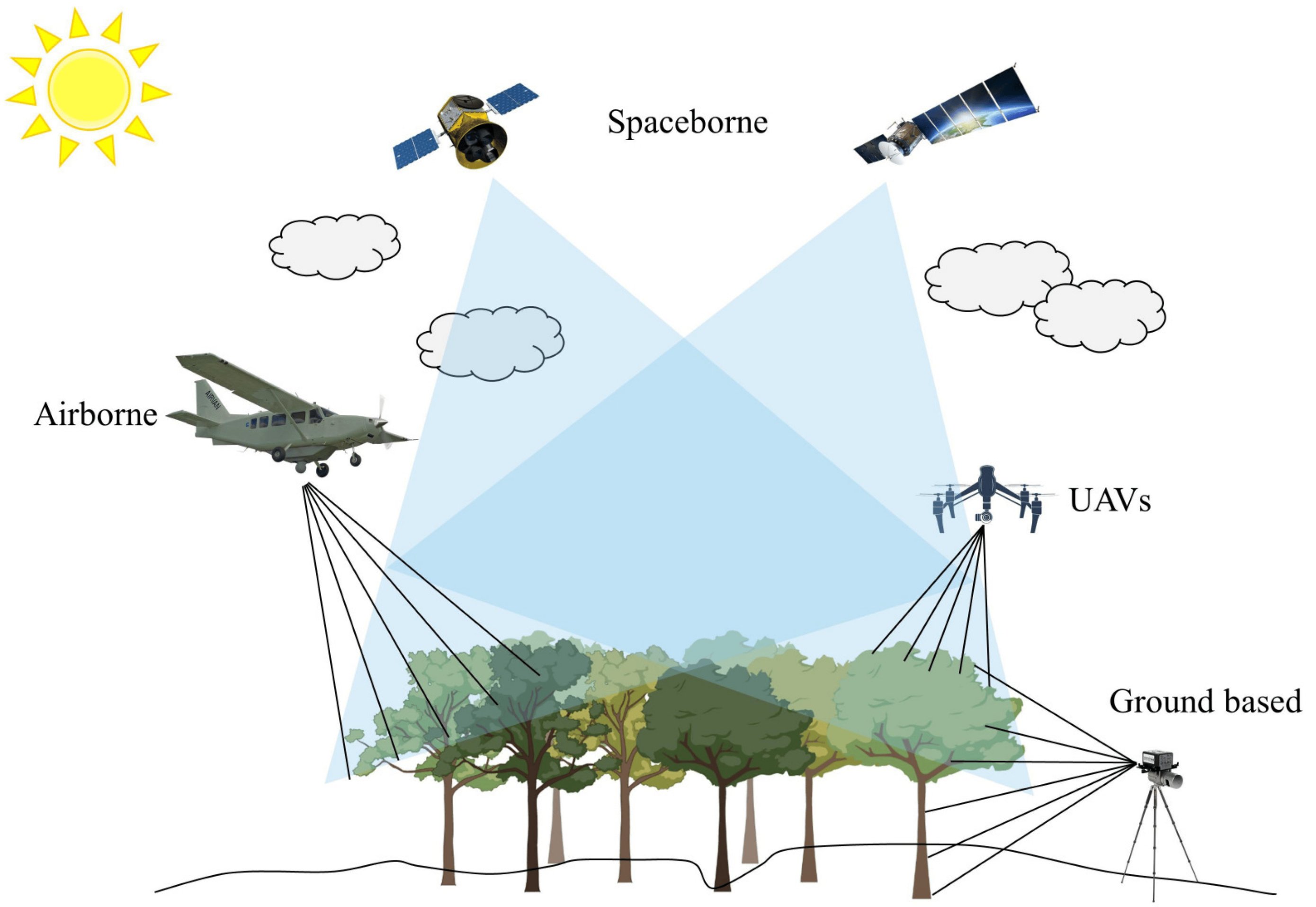

Figure 1. Illustration of forest aboveground biomass estimation using remote sensing techniques. Note: UAVs, unmanned aerial vehicles.

In addition to single-band information obtained via optical remote sensing, AGB estimations are commonly obtained using VIs based on live green vegetation absorbing solar radiation in red wavelengths to support photosynthesis, which include the normalized difference vegetation index (NDVI), difference vegetation index (DVI), and enhanced vegetation index (EVI) [18][74][75]. However, as green vegetation increases, the strong absorption of red wavelengths leads to a saturation effect, thereby decreasing the AGB estimation accuracy [36]. Nonetheless, several VIs, such as the renormalized DVI (RNDVI) and modified simple ratio (MSR), have been developed to improve the accuracy of biomass estimation in dense vegetation areas [76][77]. For sparse vegetation covers, the orthogonal transform-based perpendicular VI (PVI), soil-adjusted VI (SAVI), and modified SAVI (MSAVI) are used to minimize interference from the atmosphere and soil background [78][79][80]. Moreover, remote sensing-derived texture information has been increasingly used in the estimation of forest AGB [81][82].

Additional parameters that are essential for AGB estimation include those describing the forest structure, such as tree height, diameter at breast height (DBH), and canopy height. Tree height not only reflects the biological characteristics and growth capacity of trees, but also indicates the stand quality [83]. Previous studies have demonstrated a constant AGB-to-tree height ratio (10.6 t/(hm^2·m)) in closed-canopy forests using global sampling site survey data on forest age and average tree height [84]. In other words, the density of AGB per forest space was constant (1.0 kg/m^3). This phenomenon (called constant aboveground biomass per forest space, BPS) was more pronounced between regions, demonstrating a small mean variation of 9.4–10.5 Mg/(hm^2·m) and a global mean value of 9.9 Mg/(hm^2·m) [84]. However, it is difficult to determine tree height at the plot scale, especially in tall and closed-canopy forests; therefore, it is often more practical to determine the tree height of only some individuals and then estimate the overall tree height by establishing a growth correlation between tree height and DBH [83]. Furthermore, the power law allometric equation of AGB and tree height constructed at the plot scale remains applicable on a large scale [85], which is a significant advantage of estimating AGB using remote sensing combined with ground measurements [25][36][50]. In recent years, microwave and LiDAR remote sensing have been widely used to estimate AGB. Tree height can be accurately and conveniently obtained from InSAR and LiDAR data, which has significant potential for advancement [86][87][88]. In addition, canopy height has been shown to provide accurate AGB estimations [89][90]. Notably, canopy height is not tree height; it depends not only on tree height, but also on the canopy and stand density of each tree [36].

LAI and forest coverage are also valuable indicators for estimating AGB [52][91]. LAI refers to the total area of plant leaves per unit land area as a multiple of the land area; thus, it mainly reflects leaf biomass [92]. At large scales, LAI-based estimation of AGB requires preliminary establishment of the relationship between leaf biomass and AGB, whereafter AGB is obtained via extrapolation [93]. At small scales, however, total AGB usually refers to the sum of the wood and foliage biomass [94]. Forest coverage refers to the vertical projection of the aboveground portion of trees as a percentage of the sample area and is commonly used for closed-canopy forests to express the tree layer coverage, which is the ratio of the area covered by the forest canopy to the ground surface area [83]. Generally, in uniform forests, a higher coverage represents a higher biomass [52]. Nevertheless, as forest coverage approaches saturation (reaching 1), biomass may continue to increase, which, to some extent, reduces the biomass estimation accuracy in high forest coverage areas [36].

After solar radiation-induced excitation, green leaves emit solar-induced chlorophyll fluorescence (SIF), an electromagnetic signal in the red and far-red spectral portions, from the core of their photosynthetic machinery. Therefore, SIF is mechanically connected to photosynthesis and thus provides a better representation of vegetation growth conditions compared to other biophysical parameters or VIs [95]. Previous studies have found that SIF is strongly related to the gross primary production (GPP) [96][97][98], and GPP can provide direct AGB estimations. Therefore, GPP can be obtained via SIF–GPP correlation analyses, whereafter forest AGB can be estimated from the GPP data [18][98][99][100]. Currently, several global SIF products are available that permit forest biomass estimations [101], including the SIF datasets of Global Monitoring Ozone Experiment 2 (GOME-2) [102][103][104], Orbiting Carbon Observatory 2 (OCO-2) [105] and the Chinese Carbon Dioxide Observation Satellite (TanSat) [106]. Despite the low spatial resolution (40 km × 40 km at best) of the GOME-2 SIF dataset, it is the most widely used owing to its continuous spatial sampling, global coverage, and long time series. For example, Hu et al. [107]

developed a method to upscale SIF from instantaneous clear-sky observations to all-sky sums, adopting the absorbed photosynthetically active radiation (APAR) to correct for the effect of clouds on SIF, thereby deriving all-sky SIF (ASSIF) products from GOME-2 in 8-day and monthly intervals during 2007 and 2018. Moreover, a good correspondence between the temporal trajectories of SIF and GPP [108] has been demonstrated on a global scale by Li et al. [109], who assessed OCO-2-detected SIF data and flux tower GPP data. They showed that a strong relationship between SIF and GPP exists at the ecosystem level and is nearly universal across various biomes. Nevertheless, when using SIF data to estimate GPP and AGB, the influence of environmental conditions and vegetation structure must be considered. Accordingly, SIF yields may be less sensitive than photosynthetic yields under stress conditions [110]; and the relationship between photosynthesis and top-of-canopy SIF measurements is complicated by leaf and plant structural effects [111].

Overall, forest AGB is estimated using remotely sensed data acquired over a broad electromagnetic wavelength range, from visible light to microwaves. In addition to the above ecological process parameters, environmental (e.g., precipitation, temperature, and atmospheric pressure), topographic (e.g., elevation and slope), and biotic (e.g., species diversity) factors also affect forest AGB estimates. Specifically, factors such as precipitation, temperature, elevation, and slope drive tree species distribution patterns, while soil resources and radiation intensity determine vegetation growth conditions, all of which influence forest AGB [112]. In addition, by taking succession, disturbance, and ecosystem processes into account, forest AGB estimation accuracy may be improved [36][113].

References

1. Nerem, R.S.; Beckley, B.D.; Fasullo, J.T.; Hamlington, B.D.; Masters, D.; Mitchum, G.T. Climate-change-driven accelerated sea-level rise detected in the altimeter era. Proc. Natl. Acad. Sci. USA 2018, 115, 2022–2025.
2. Radic, V.; Bliss, A.; Beedlow, A.C.; Hock, R.; Miles, E.; Cogley, J.G. Regional and global projections of twenty-first century glacier mass changes in response to climate scenarios from global climate models. Clim. Dynam. 2014, 42, 37–58.
3. Zheng, G.X.; Allen, S.K.; Bao, A.; Ballesteros-Canovas, J.A.; Huss, M.; Zhang, G.Q.; Li, J.L.; Yuan, Y.; Jiang, L.L.; Yu, T.; et al. Increasing risk of glacial lake outburst floods from future Third Pole deglaciation. Nat. Clim. Change 2021, 11, 411–417.
4. Kang, S.C.; Zhang, Q.G.; Qian, Y.; Ji, Z.M.; Li, C.L.; Cong, Z.Y.; Zhang, Y.L.; Guo, J.M.; Du, W.T.; Huang, J.; et al. Linking atmospheric pollution to cryospheric change in the Third Pole region: Current progress and future prospects. Natl. Sci. Rev. 2019, 6, 796–809.
5. Yin, J.B.; Gentine, P.; Zhou, S.; Sullivan, S.C.; Wang, R.; Zhang, Y.; Guo, S.L. Large increase in global storm runoff extremes driven by climate and anthropogenic changes. Nat. Commun. 2018, 9, 4389.

6. Ebi, K.L.; Vanos, J.; Baldwin, J.W.; Bell, J.E.; Hondula, D.M.; Errett, N.A.; Hayes, K.; Reid, C.E.; Saha, S.; Spector, J.; et al. Extreme Weather and Climate Change: Population Health and Health System Implications. In Annual Review of Public Health; Fielding, J.E., Ed.; Annual Review of Public Health: San Mateo, CA, USA, 2021; Volume 42, pp. 293–315.
7. Hasegawa, T.; Fujimori, S.; Havlik, P.; Valin, H.; Bodirsky, B.L.; Doelman, J.C.; Fellmann, T.; Kyle, P.; Koopman, J.F.L.; Lotze-Campen, H.; et al. Risk of increased food insecurity under stringent global climate change mitigation policy. Nat. Clim. Change 2018, 8, 699–703.
8. Bellard, C.; Bertelsmeier, C.; Leadley, P.; Thuiller, W.; Courchamp, F. Impacts of climate change on the future of biodiversity. Ecol. Lett. 2012, 15, 365–377.
9. Frumkin, H.; Haines, A. Global Environmental Change and Noncommunicable Disease Risks. In Annual Review of Public Health; Fielding, J.E., Ed.; Annual Review of Public Health: San Mateo, CA, USA, 2019; Volume 40, pp. 261–282.
10. Gosling, S.N.; Arnell, N.W. A global assessment of the impact of climate change on water scarcity. Clim. Change 2016, 134, 371–385.
11. Hoegh-Guldberg, O.; Jacob, D.; Taylor, M.; Guillen Bolanos, T.; Bindi, M.; Brown, S.; Camilloni, I.; Diedhiou, A.; Djalante, R.; Ebi, K.; et al. The human imperative of stabilizing global climate change at 1.5 °C. Science 2019, 365, 1263.
12. Sippel, S.; Meinshausen, N.; Fischer, E.M.; Szekely, E.; Knutti, R. Climate change now detectable from any single day of weather at global scale. Nat. Clim. Change 2020, 10, 35–41.
13. Pan, Y.D.; Birdsey, R.A.; Fang, J.Y.; Houghton, R.; Kauppi, P.E.; Kurz, W.A.; Phillips, O.L.; Shvidenko, A.; Lewis, S.L.; Canadell, J.G.; et al. A Large and Persistent Carbon Sink in the World’s Forests. Science 2011, 333, 988–993.
14. Houghton, R.A.; Hall, F.; Goetz, S.J. Importance of biomass in the global carbon cycle. J. Geophys. Res.-Biogeosci. 2009, 114, G00E03.
15. Molotoks, A.; Stehfest, E.; Doelman, J.; Albanito, F.; Fitton, N.; Dawson, T.P.; Smith, P. Global projections of future cropland expansion to 2050 and direct impacts on biodiversity and carbon storage. Glob. Change Biol. 2018, 24, 5895–5908.
16. Tian, L.; Tao, Y.; Fu, W.X.; Li, T.; Ren, F.; Li, M.Y. Dynamic Simulation of Land Use/Cover Change and Assessment of Forest Ecosystem Carbon Storage under Climate Change Scenarios in Guangdong Province, China. Remote Sens. 2022, 14, 2330.
17. Payne, N.J.; Cameron, D.A.; Leblanc, J.D.; Morrison, I.K. Carbon storage and net primary productivity in Canadian boreal mixedwood stands. J. For. Res. 2019, 30, 1667–1678.
18. Xiao, J.F.; Chevallier, F.; Gomez, C.; Guanter, L.; Hicke, J.A.; Huete, A.R.; Ichii, K.; Ni, W.J.; Pang, Y.; Rahman, A.F.; et al. Remote sensing of the terrestrial carbon cycle: A review of advances over

50 years. Remote Sens. Environ. 2019, 233, 111383.

19. Chave, J.; Rejou-Mechain, M.; Burquez, A.; Chidumayo, E.; Colgan, M.S.; Delitti, W.B.; Duque, A.; Eid, T.; Fearnside, P.M.; Goodman, R.C.; et al. Improved allometric models to estimate the aboveground biomass of tropical trees. Glob. Change Biol. 2014, 20, 3177–3190.
20. Chang, F.C.; Ko, C.H.; Yang, P.Y.; Chen, K.S.; Chang, K.H. Carbon sequestration and substitution potential of subtropical mountain Sugi plantation forests in central Taiwan. J. Clean. Prod. 2017, 167, 1099–1105.
21. Li, D.R.; Wang, C.W.; Hu, Y.M.; Liu, S.G. General Review on Remote Sensing-Based Biomass Estimation. Geomat. Inform. Sci. Wuhan Univ. 2012, 37, 631–635.
22. Brown, S.; Sathaye, J.; Cannell, M.; Kauppi, P.E. Mitigation of carbon emissions to the atmosphere by forest management. Commonw. For. Rev. 1996, 75, 80–91.
23. Lu, D.S.; Batistella, M.; Moran, E. Satellite estimation of aboveground biomass and impacts of forest stand structure. Photogramm. Eng. Remote Sens. 2005, 71, 967–974.
24. Zhang, Z.; Tian, X.; Chen, R.X.; He, Q.S. Review of methods on estimating forest above ground biomass. J. Beijing For. Univ. 2011, 33, 144–150.
25. Huang, H.B.; Liu, C.X.; Wang, X.Y.; Zhou, X.L.; Gong, P. Integration of multi-resource remotely sensed data and allometric models for forest aboveground biomass estimation in China. Remote Sens. Environ. 2019, 221, 225–234.
26. Myneni, R.B.; Dong, J.; Tucker, C.J.; Kaufmann, R.K.; Kauppi, P.E.; Liski, J.; Zhou, L.; Alexeyev, V.; Hughes, M.K. A large carbon sink in the woody biomass of Northern forests. Proc. Natl. Acad. Sci. USA 2001, 98, 14784–14789.
27. Nelson, R.; Gobakken, T.; Naesset, E.; Gregoire, T.G.; Stahl, G.; Holm, S.; Flewelling, J. Lidar sampling—Using an airborne profiler to estimate forest biomass in Hedmark County, Norway. Remote Sens. Environ. 2012, 123, 563–578.
28. Houghton, R.A. Aboveground Forest Biomass and the Global Carbon Balance. Glob. Change Biol. 2005, 11, 945–958.
29. Li, Y.C.; Li, C.; Li, M.Y.; Liu, Z.Z. Influence of Variable Selection and Forest Type on Forest Aboveground Biomass Estimation Using Machine Learning Algorithms. Forests 2019, 10, 1073.
30. Zhang, R.; Zhou, X.H.; Ouyang, Z.T.; Avitabile, V.; Qi, J.G.; Chen, J.Q.; Giannico, V. Estimating aboveground biomass in subtropical forests of China by integrating multisource remote sensing and ground data. Remote Sens. Environ. 2019, 232, 111341.
31. Narine, L.L.; Popescu, S.; Neuenschwander, A.; Zhou, T.; Srinivasan, S.; Harbeck, K. Estimating aboveground biomass and forest canopy cover with simulated ICESat-2 data. Remote Sens. Environ. 2019, 224, 1–11.

32. Fan, W.Y.; Li, M.Z.; Yang, J.M. Forest Biomass Estimation Models of Remote Sensing in Changbai Mountain Forests. Sci. Silvae Sinicae 2011, 47, 16–20.
33. Sarker, M.L.R.; Nichol, J.; Iz, H.B.; Bin Ahmad, B.; Rahman, A.A. Forest Biomass Estimation Using Texture Measurements of High-Resolution Dual-Polarization C-Band SAR Data. IEEE Trans. Geosci. Remote 2013, 51, 3371–3384.
34. Ali, A.; Lin, S.L.; He, J.K.; Kong, F.M.; Yu, J.H.; Jiang, H.S. Climate and soils determine aboveground biomass indirectly via species diversity and stand structural complexity in tropical forests. For. Ecol. Manag. 2019, 432, 823–831.
35. Deng, L.; Liu, S.G.; Kim, D.G.; Peng, C.H.; Sweeney, S.; Shangguan, Z.P. Past and future carbon sequestration benefits of China's grain for green program. Glob. Environ. Change 2017, 47, 13–20.
36. Zhang, Y.Z.; Liang, S.L.; Yang, L. A Review of Regional and Global Gridded Forest Biomass Datasets. Remote Sens. 2019, 11, 2744.
37. Cartus, O.; Santoro, M.; Kellndorfer, J. Mapping forest aboveground biomass in the Northeastern United States with ALOS PALSAR dual-polarization L-band. Remote Sens. Environ. 2012, 124, 466–478.
38. Ketterings, Q.M.; Coe, R.; van Noordwijk, M.; Ambagau, Y.; Palm, C.A. Reducing uncertainty in the use of allometric biomass equations for predicting above-ground tree biomass in mixed secondary forests. For. Ecol. Manag. 2001, 146, 199–209.
39. Kenzo, T.; Furutani, R.; Hattori, D.; Kendawang, J.J.; Tanaka, S.; Sakurai, K.; Ninomiya, I. Allometric equations for accurate estimation of above-ground biomass in logged-over tropical rainforests in Sarawak, Malaysia. J. For. Res. 2009, 14, 365–372.
40. Lu, D.S.; Chen, Q.; Wang, G.X.; Liu, L.J.; Li, G.Y.; Moran, E. A survey of remote sensing-based aboveground biomass estimation methods in forest ecosystems. Int. J. Digit. Earth 2016, 9, 63–105.
41. Saatchi, S.S.; Houghton, R.A.; Alvala, R.; Soares, J.V.; Yu, Y. Distribution of aboveground live biomass in the Amazon basin. Global Change Biol. 2007, 13, 816–837.
42. Baccini, A.; Goetz, S.J.; Walker, W.S.; Laporte, N.T.; Sun, M.; Sulla-Menashe, D.; Hackler, J.; Beck, P.S.A.; Dubayah, R.; Friedl, M.A.; et al. Estimated carbon dioxide emissions from tropical deforestation improved by carbon-density maps. Nat. Clim. Change 2012, 2, 182–185.
43. Badreldin, N.; Sanchez-Azofeifa, A. Estimating Forest Biomass Dynamics by Integrating Multi-Temporal Landsat Satellite Images with Ground and Airborne LiDAR Data in the Coal Valley Mine, Alberta, Canada. Remote Sens. 2015, 7, 2832–2849.

44. Bouvet, A.; Mermoz, S.; Toan, T.L.; Villard, L.; Mathieu, R.; Naidoo, L.; Asner, G.P. An above-ground biomass map of African savannahs and woodlands at 25 m resolution derived from ALOS PALSAR. Remote Sens. Environ. 2018, 206, 156–173.

45. Santoro, M.; Beaudoin, A.; Beer, C.; Cartus, O.; Fransson, J.B.S.; Hall, R.J.; Pathe, C.; Schmullius, C.; Schepaschenko, D.; Shvidenko, A.; et al. Forest growing stock volume of the northern hemisphere: Spatially explicit estimates for 2010 derived from Envisat ASAR. Remote Sens. Environ. 2015, 168, 316–334.

46. Tian, X.; Yan, M.; van der Tol, C.; Li, Z.; Su, Z.B.; Chen, E.X.; Li, X.; Li, L.H.; Wang, X.F.; Pan, X.D.; et al. Modeling forest above-ground biomass dynamics using multi-source data and incorporated models: A case study over the qilian mountains. Agric. For. Meteorol. 2017, 246, 1–14.

47. Hurtt, G.C.; Fisk, J.; Thomas, R.Q.; Dubayah, R.; Moorcroft, P.R.; Shugart, H.H. Linking models and data on vegetation structure. J. Geophys. Res.-Biogeosci. 2010, 115, G00E10.

48. Waring, R.H.; Coops, N.C.; Landsberg, J.J. Improving predictions of forest growth using the 3-PGS model with observations made by remote sensing. For. Ecol. Manag. 2010, 259, 1722–1729.

49. Yan, F.; Wu, B.; Wang, Y.J. Estimating spatiotemporal patterns of aboveground biomass using Landsat TM and MODIS images in the Mu Us Sandy Land, China. Agric. For. Meteorol. 2015, 200, 119–128.

50. Chopping, M.; Wang, Z.S.; Schaaf, C.; Bull, M.A.; Duchesne, R.R. Forest aboveground biomass in the southwestern United States from a MISR multi-angle index, 2000–2015. Remote Sens. Environ. 2022, 275, 112964.

51. Foody, G.M.; Boyd, D.S.; Cutler, M.E.J. Predictive relations of tropical forest biomass from Landsat TM data and their transferability between regions. Remote Sens. Environ. 2003, 85, 463–474.

52. Blackard, J.A.; Finco, M.V.; Helmer, E.H.; Holden, G.R.; Hoppus, M.L.; Jacobs, D.M.; Lister, A.J.; Moisen, G.G.; Nelson, M.D.; Riemann, R.; et al. Mapping US forest biomass using nationwide forest inventory data and moderate resolution information. Remote Sens. Environ. 2008, 112, 1658–1677.

53. Baccini, A.; Walker, W.; Carvalho, L.; Farina, M.; Sulla-Menashe, D.; Houghton, R.A. Tropical forests are a net carbon source based on aboveground measurements of gain and loss. Science 2017, 358, 230–233.

54. Beaudoin, A.; Bernier, P.Y.; Guindon, L.; Villemaire, P.; Guo, X.J.; Stinson, G.; Bergeron, T.; Magnussen, S.; Hall, R.J. Mapping attributes of Canada’s forests at moderate resolution through kNN and MODIS imagery. Can. J. For. Res. 2014, 44, 521–532.

55. Dube, T.; Mutanga, O. Evaluating the utility of the medium-spatial resolution Landsat 8 multispectral sensor in quantifying aboveground biomass in uMgeni catchment, South Africa. ISPRS J. Photogramm. 2015, 101, 36–46.

56. Hall, R.J.; Skakun, R.S.; Arsenault, E.J.; Case, B.S. Modeling forest stand structure attributes using Landsat ETM+ data: Application to mapping of aboveground biomass and stand volume. For. Ecol. Manag. 2006, 225, 378–390.

57. Powell, S.L.; Cohen, W.B.; Healey, S.P.; Kennedy, R.E.; Moisen, G.G.; Pierce, K.B.; Ohmann, J.L. Quantification of live aboveground forest biomass dynamics with Landsat time-series and field inventory data: A comparison of empirical modeling approaches. Remote Sens. Environ. 2010, 114, 1053–1068.

58. Fremout, T.; Vinatea, J.C.D.; Thomas, E.; Huaman-Zambrano, W.; Salazar-Villegas, M.; de la Fuente, D.L.; Bernardino, P.N.; Atkinson, R.; Csaplovics, E.; Muys, B. Site-specific scaling of remote sensing-based estimates of woody cover and aboveground biomass for mapping long-term tropical dry forest degradation status. Remote Sens. Environ. 2022, 276, 113040.

59. Dillabaugh, K.A.; King, D.J. Riparian marshland composition and biomass mapping using Ikonos imagery. Can. J. Remote Sens. 2008, 34, 143–158.

60. Eckert, S. Improved Forest Biomass and Carbon Estimations Using Texture Measures from WorldView-2 Satellite Data. Remote Sens. 2012, 4, 810–829.

61. Hirata, Y.; Tabuchi, R.; Patanaponpaiboon, P.; Poungparn, S.; Yoneda, R.; Fujioka, Y. Estimation of aboveground biomass in mangrove forests using high-resolution satellite data. J. For. Res. 2014, 19, 34–41.

62. Cartus, O.; Kellndorfer, J.; Walker, W.; Franco, C.; Bishop, J.; Santos, L.; Fuentes, J.M.M. A National, Detailed Map of Forest Aboveground Carbon Stocks in Mexico. Remote Sens. 2014, 6, 5559–5588.

63. Yu, Y.F.; Saatchi, S. Sensitivity of L-Band SAR Backscatter to Aboveground Biomass of Global Forests. Remote Sens. 2016, 8, 522.

64. Pham, T.D.; Yokoya, N.; Bui, D.T.; Yoshino, K.; Friess, D.A. Remote Sensing Approaches for Monitoring Mangrove Species, Structure, and Biomass: Opportunities and Challenges. Remote Sens. 2019, 11, 230.

65. Luo, H.M.; Chen, R.X.; Li, Z.Y.; Cao, C.X. Forest baove ground biomass estimation methodology based on polarization coherence tomography. Natl. Remote Sens. Bull. 2011, 15, 1138–1155.

66. Li, W.M.; Chen, R.X.; Li, Z.Y.; Zhao, L. Forest Above-Ground Biomass Estimation Using Polarimetric Interferometry SAR Coherence Tomography. Sci. Silvae Sinicae 2014, 50, 70–77.

67. Zhao, P.P.; Lu, D.S.; Wang, G.X.; Wu, C.P.; Huang, Y.J.; Yu, S.Q. Examining Spectral Reflectance Saturation in Landsat Imagery and Corresponding Solutions to Improve Forest Aboveground Biomass Estimation. Remote Sens. 2016, 8, 469.
68. Baccini, A.; Asner, G.P. Improving pantropical forest carbon maps with airborne LiDAR sampling. Carbon Manag. 2013, 4, 591–600.
69. Asner, G.P.; Mascaro, J.; Anderson, C.; Knapp, D.E.; Martin, R.E.; Kennedy-Bowdoin, T.; van Breugel, M.; Davies, S.; Hall, J.S.; Muller-Landau, H.C.; et al. High-fidelity national carbon mapping for resource management and REDD+. Carbon Bal. Manag. 2013, 8, 7.
70. Poley, L.G.; McDermid, G.J. A Systematic Review of the Factors Influencing the Estimation of Vegetation Aboveground Biomass Using Unmanned Aerial Systems. Remote Sens. 2020, 12, 1052.
71. Fan, X.Y.; Kawamura, K.; Xuan, T.D.; Yuba, N.; Lim, J.; Yoshitoshi, R.; Minh, T.N.; Kurokawa, Y.; Obitsu, T. Low-cost visible and near-infrared camera on an unmanned aerial vehicle for assessing the herbage biomass and leaf area index in an Italian ryegrass field. Grassl. Sci. 2018, 64, 145–150.
72. Schirrmann, M.; Giebel, A.; Gleiniger, F.; Pflanz, M.; Lentschke, J.; Dammer, K.H. Monitoring Agronomic Parameters of Winter Wheat Crops with Low-Cost UAV Imagery. Remote Sens. 2016, 8, 706.
73. Doughty, C.L.; Cavanaugh, K.C. Mapping Coastal Wetland Biomass from High Resolution Unmanned Aerial Vehicle (UAV) Imagery. Remote Sens. 2019, 11, 540.
74. Garroutte, E.L.; Hansen, A.J.; Lawrence, R.L. Using NDVI and EVI to Map Spatiotemporal Variation in the Biomass and Quality of Forage for Migratory Elk in the Greater Yellowstone Ecosystem. Remote Sens. 2016, 8, 404.
75. Tian, F.; Brandt, M.; Liu, Y.Y.; Verger, A.; Tagesson, T.; Diouf, A.A.; Rasmussen, K.; Mbow, C.; Wang, Y.J.; Fensholt, R. Remote sensing of vegetation dynamics in drylands: Evaluating vegetation optical depth (VOD) using AVHRR NDVI and in situ green biomass data over West African Sahel. Remote Sens. Environ. 2016, 177, 265–276.
76. Durante, P.; Martín-Alcón, S.; Gil-Tena, A.; Algeet, N.; Tomé, J.L.; Recuero, L.; Palacios-Orueta, A.; Oyonarte, C. Improving Aboveground Forest Biomass Maps: From High-Resolution to National Scale. Remote Sens. 2019, 11, 795.
77. Chen, J.M. Evaluation of Vegetation Indices and a Modified Simple Ratio for Boreal Applications. Can. J. Remote Sens. 1996, 22, 229–242.
78. Fatehi, P.; Damm, A.; Schaepman, M.E.; Kneubuhler, M. Estimation of Alpine Forest Structural Variables from Imaging Spectrometer Data. Remote Sens. 2015, 7, 16315–16338.

79. Luo, S.Z.; Wang, C.; Xi, X.H.; Pan, F.F.; Qian, M.J.; Peng, D.L.; Nie, S.; Qin, H.M.; Lin, Y. Retrieving aboveground biomass of wetland Phragmites australis (common reed) using a combination of airborne discrete-return LiDAR and hyperspectral data. Int. J. Appl. Earth Obs. 2017, 58, 107–117.
80. Sadeghi, Y.; St-Onge, B.; Leblon, B.; Prieur, J.F.; Simard, M. Mapping boreal forest biomass from a SRTM and TanDEM-X based on canopy height model and Landsat spectral indices. Int. J. Appl. Earth Obs. 2018, 68, 202–213.
81. Kelsey, K.C.; Neff, J.C. Estimates of Aboveground Biomass from Texture Analysis of Landsat Imagery. Remote Sens. 2014, 6, 6407–6422.
82. Sarker, L.R.; Nichol, J.E. Improved forest biomass estimates using ALOS AVNIR-2 texture indices. Remote Sens. Environ. 2011, 115, 968–977.
83. Fang, J.Y.; Zhu, J.X.; Li, P.; Ji, C.J.; Zhu, J.L.; Jiang, L.; Chen, G.P.; Cai, Q.; Su, H.J.; Feng, Y.H.; et al. Carbon Budgets of Forest Ecosystems in China; Science Press: Beijing, China, 2021.
84. Fang, J.Y.; Brown, S.; Tang, Y.H.; Nabuurs, G.J.; Wang, X.P.; Shen, H.H. Overestimated biomass carbon pools of the northern mid- and high latitude forests. Clim. Change 2006, 74, 355–368.
85. Wu, X.; Wang, X.P.; Wu, Y.L.; Xia, X.L.; Fang, J.Y. Forest biomass is strongly shaped by forest height across boreal to tropical forests in China. J. Plant Ecol. 2015, 8, 559–567.
86. Solberg, S.; Nasset, E.; Gobakken, T.; Bollandsas, O.-M. Forest biomass change estimated from height change in interferometric SAR height models. Carbon Bal. Manag. 2014, 9, 5.
87. Yu, Y.F.; Saatchi, S.; Heath, L.S.; LaPoint, E.; Myneni, R.; Knyazikhin, Y. Regional distribution of forest height and biomass from multisensor data fusion. J. Geophys. Res.-Biogeosci. 2010, 115, G00E12.
88. Asner, G.P.; Mascaro, J. Mapping tropical forest carbon: Calibrating plot estimates to a simple LiDAR metric. Remote Sens. Environ. 2014, 140, 614–624.
89. Simard, M.; Fatoyinbo, L.; Smetanka, C.; Rivera-Monroy, V.H.; Castaneda-Moya, E.; Thomas, N.; Van der Stocken, T. Mangrove canopy height globally related to precipitation, temperature and cyclone frequency. Nat. Geosci. 2019, 12, 40–45.
90. Bouvier, M.; Durrieu, S.; Fournier, R.A.; Renaud, J.P. Generalizing predictive models of forest inventory attributes using an area-based approach with airborne LiDAR data. Remote Sens. Environ. 2015, 156, 322–334.
91. Zhang, G.; Ganguly, S.; Nemani, R.R.; White, M.A.; Milesi, C.; Hashimoto, H.; Wang, W.L.; Saatchi, S.; Yu, Y.F.; Myneni, R.B. Estimation of forest aboveground biomass in California using canopy height and leaf area index estimated from satellite data. Remote Sens. Environ. 2014, 151, 44–56.

92. Wu, Y.C.; Strahler, A.H. Remote estimation of crown size, stand density, and biomass on the Oregon transect. Ecol. Appl. 1994, 4, 299–312.
93. Zhang, X.Y.; Kondragunta, S. Estimating forest biomass in the USA using generalized allometric models and MODIS land products. Geophys. Res. Lett. 2006, 33, L09402.
94. Berner, L.T.; Law, B.E. Plant traits, productivity, biomass and soil properties from forest sites in the Pacific Northwest, 1999–2014. Sci. Data 2016, 3, 160002.
95. Porcar-Castell, A.; Tyystjarvi, E.; Atherton, J.; van der Tol, C.; Flexas, J.; Pfundel, E.E.; Moreno, J.; Frankenberg, C.; Berry, J.A. Linking chlorophyll a fluorescence to photosynthesis for remote sensing applications: Mechanisms and challenges. J. Exp. Bot. 2014, 65, 4065–4095.
96. Gu, L.; Wood, J.D.; Chang, C.Y.Y.; Sun, Y.; Riggs, J.S. Advancing Terrestrial Ecosystem Science with a Novel Automated Measurement System for Sun-Induced Chlorophyll Fluorescence for Integration with Eddy Covariance Flux Networks. J. Geophys. Res.-Biogeosci. 2019, 124, 127–146.
97. Damm, A.; Guanter, L.; Paul-Limoges, E.; van der Tol, C.; Hueni, A.; Buchmann, N.; Eugster, W.; Ammann, C.; Schaepman, M.E. Far-red sun-induced chlorophyll fluorescence shows ecosystem-specific relationships to gross primary production: An assessment based on observational and modeling approaches. Remote Sens. Environ. 2015, 166, 91–105.
98. Yang, K.; Ryu, Y.; Dechant, B.; Berry, J.A.; Hwang, Y.; Jiang, C.; Kang, M.; Min, J.; Kimm, H.; Kornfeld, A.; et al. Sun-induced chlorophyll fluorescence is more strongly related to absorbed light than to photosynthesis at half-hourly resolution in a rice paddy. Remote Sens. Environ. 2018, 216, 658–673.
99. Qin, Y.W.; Xiao, X.M.; Wigneron, J.P.; Ciais, P.; Canadell, J.G.; Brandt, M.; Li, X.J.; Fan, L.; Wu, X.C.; Tang, H.; et al. Large loss and rapid recovery of vegetation cover and aboveground biomass over forest areas in Australia during 2019–2020. Remote Sens. Environ. 2022, 278, 113087.
100. Yang, X.; Tang, J.W.; Mustard, J.F.; Lee, J.E.; Rossini, M.; Joiner, J.; Munger, J.W.; Kornfeld, A.; Richardson, A.D. Solar-induced chlorophyll fluorescence that correlates with canopy photosynthesis on diurnal and seasonal scales in a temperate deciduous forest. Geophys. Res. Lett. 2015, 42, 2977–2987.
101. Frankenberg, C.; Fisher, J.B.; Worden, J.; Badgley, G.; Saatchi, S.S.; Lee, J.E.; Toon, G.C.; Butz, A.; Jung, M.; Kuze, A.; et al. New global observations of the terrestrial carbon cycle from GOSAT: Patterns of plant fluorescence with gross primary productivity. Geophys. Res. Lett. 2011, 38, L17706.
102. Kohler, P.; Guanter, L.; Joiner, J. A linear method for the retrieval of sun-induced chlorophyll fluorescence from GOME-2 and SCIAMACHY data. Atmos. Meas. Tech. 2015, 8, 2589–2608.

103. Joiner, J.; Yoshida, Y.; Vasilkov, A.P.; Middleton, E.M.; Campbell, P.K.E.; Yoshida, Y.; Kuze, A.; Corp, L.A. Filling-in of near-infrared solar lines by terrestrial fluorescence and other geophysical effects: Simulations and space-based observations from SCIAMACHY and GOSAT. Atmos. Meas. Tech. 2012, 5, 809–829.

104. Wolanin, A.; Rozanov, V.V.; Dinter, T.; Noel, S.; Vountas, M.; Burrows, J.P.; Bracher, A. Global retrieval of marine and terrestrial chlorophyll fluorescence at its red peak using hyperspectral top of atmosphere radiance measurements: Feasibility study and first results. Remote Sens. Environ. 2015, 166, 243–261.

105. Sun, Y.; Frankenberg, C.; Jung, M.; Joiner, J.; Guanter, L.; Kohler, P.; Magney, T. Overview of Solar-Induced chlorophyll Fluorescence (SIF) from the Orbiting Carbon Observatory-2: Retrieval, cross-mission comparison, and global monitoring for GPP. Remote Sens. Environ. 2018, 209, 808–823.

106. Du, S.S.; Liu, L.Y.; Liu, X.J.; Zhang, X.; Zhang, X.Y.; Bi, Y.M.; Zhang, L.C. Retrieval of global terrestrial solar-induced chlorophyll fluorescence from TanSat satellite. Sci. Bull. 2018, 63, 1502–1512.

107. Hu, J.C.; Liu, L.Y.; Yu, H.Y.; Guan, L.L.; Liu, X.J. Upscaling GOME-2 SIF from clear-sky instantaneous observations to all-sky sums leading to an improved SIF-GPP correlation. Agric. For. Meteorol. 2021, 306, 108439.

108. Joiner, J.; Yoshida, Y.; Vasilkov, A.; Schaefer, K.; Jung, M.; Guanter, L.; Zhang, Y.; Garrity, S.; Middleton, E.M.; Huemmrich, K.F.; et al. The seasonal cycle of satellite chlorophyll fluorescence observations and its relationship to vegetation phenology and ecosystem atmosphere carbon exchange. Remote Sens. Environ. 2014, 152, 375–391.

109. Li, X.; Xiao, J.F.; He, B.B.; Arain, M.A.; Beringer, J.; Desai, A.R.; Emmel, C.; Hollinger, D.Y.; Krasnova, A.; Mammarella, I.; et al. Solar-induced chlorophyll fluorescence is strongly correlated with terrestrial photosynthesis for a wide variety of biomes: First global analysis based on OCO-2 and flux tower observations. Glob. Change Biol. 2018, 24, 3990–4008.

110. Wohlfahrt, G.; Gerdel, K.; Migliavacca, M.; Rotenberg, E.; Tatarinov, F.; Müller, J.; Hammerle, A.; Julitta, T.; Spielmann, F.M.; Yakir, D. Sun-induced fluorescence and gross primary productivity during a heat wave. Sci. Rep. 2018, 8, 14169.

111. Fournier, A.; Daumard, F.; Champagne, S.; Ounis, A.; Goulas, Y.; Moya, I. Effect of canopy structure on sun-induced chlorophyll fluorescence. ISPRS J. Photogramm. 2012, 68, 112–120.

112. McEwan, R.W.; Lin, Y.C.; Sun, I.F.; Hsieh, C.F.; Su, S.H.; Chang, L.W.; Song, G.Z.M.; Wang, H.H.; Hwong, J.L.; Lin, K.C.; et al. Topographic and biotic regulation of aboveground carbon storage in subtropical broad-leaved forests of Taiwan. For. Ecol. Manag. 2011, 262, 1817–1825.

113. Frolking, S.; Palace, M.W.; Clark, D.B.; Chambers, J.Q.; Shugart, H.H.; Hurtt, G.C. Forest disturbance and recovery: A general review in the context of spaceborne remote sensing of impacts on aboveground biomass and canopy structure. J. Geophys. Res.-Biogeosci. 2009, 114, G00E02.